

Magnetic order in spin-1 and spin- $\frac{3}{2}$ interpolating square-triangle Heisenberg antiferromagnets

P. H. Y. Li and R. F. Bishop

School of Physics and Astronomy, The University of Manchester, Schuster Building, Manchester, M13 9PL, United Kingdom

Received: date / Revised version: date

Abstract. Using the coupled cluster method we investigate spin- s J_1 - J'_2 Heisenberg antiferromagnets (HAFs) on an infinite, anisotropic, two-dimensional triangular lattice for the two cases where the spin quantum number $s = 1$ and $s = \frac{3}{2}$. With respect to an underlying square-lattice geometry the model has antiferromagnetic ($J_1 > 0$) bonds between nearest neighbours and competing ($J'_2 > 0$) bonds between next-nearest neighbours across only one of the diagonals of each square plaquette, the same diagonal in each square. In a topologically equivalent triangular-lattice geometry, the model has two types of nearest-neighbour bonds: namely the $J'_2 \equiv \kappa J_1$ bonds along parallel chains and the J_1 bonds producing an inter-chain coupling. The model thus interpolates between an isotropic HAF on the square lattice at one limit ($\kappa = 0$) and a set of decoupled chains at the other limit ($\kappa \rightarrow \infty$), with the isotropic HAF on the triangular lattice in between at $\kappa = 1$. For both the spin-1 model and the spin- $\frac{3}{2}$ model we find a second-order type of quantum phase transition at $\kappa_c = 0.615 \pm 0.010$ and $\kappa_c = 0.575 \pm 0.005$ respectively, between a Néel antiferromagnetic state and a helically ordered state. In both cases the ground-state energy E and its first derivative $dE/d\kappa$ are continuous at $\kappa = \kappa_c$, while the order parameter for the transition (viz., the average ground-state on-site magnetization) does not go to zero there on either side of the transition. The phase transition at $\kappa = \kappa_c$ between the Néel antiferromagnetic phase and the helical phase for both the $s = 1$ and $s = \frac{3}{2}$ cases is analogous to that also observed in our previous work for the $s = \frac{1}{2}$ case at a value $\kappa_c = 0.80 \pm 0.01$. However, for the higher spin values the transition appears to be of continuous (second-order) type, exactly as in the classical case, whereas for the $s = \frac{1}{2}$ case it appears to be weakly first-order in nature (although a second-order transition could not be ruled out entirely).

PACS. 75.10.Jm Quantized spin models – 75.30.Kz Magnetic phase boundaries – 75.50.Ee Antiferromagnetics

1 Introduction

In recent years, the theoretical study of two-dimensional (2D) quantum spin systems has been intensely motivated by the fact that such models often describe well the properties of real magnetic materials of great experimental interest. It is an encouraging fact that experiments have often supported theoretical predictions or vice versa. Moreover, the study of frustration and quantum fluctuation in quantum spin-lattice systems has developed into an extremely active area of research. The interplay between frustration and quantum fluctuations in magnetic systems can produce a wide range of fascinating quantum phases [1, 2, 3]. Both effects are in principle capable of destabilising or completely destroying the magnetic order of the spin system. In turn this might then lead to the formation of a spin-liquid phase or be responsible for other quantum phenomena of similar significant interest. The driving force for the differentiated manifestation of the various kinds of possible quantum effects can, in principle, also come from

the type and nature of the underlying crystallographic lattice, from the number and variety of the magnetic bonds, and from the magnitude of the spin quantum numbers of the atoms that reside on the atomic lattice sites [4]. It is thus of considerable interest to try to study the effects of each of these driving forces in turn for specific model Hamiltonians.

A particularly well studied 2D model is the frustrated spin- $\frac{1}{2}$ J_1 - J_2 model on the square lattice with nearest-neighbour (NN) bonds (J_1) and next-nearest-neighbour (NNN) bonds (J_2), for which it is now well accepted that in the case where both sorts of bonds are antiferromagnetic ($J_i > 0$; $i = 1, 2$) there exist two antiferromagnetic phases exhibiting magnetic long-range order (LRO) at small and at large values of $\alpha \equiv J_2/J_1$ respectively. These are separated by an intermediate quantum paramagnetic phase without magnetic LRO in the parameter regime $\alpha_{c_1} < \alpha < \alpha_{c_2}$, where $\alpha_{c_1} \approx 0.4$ and $\alpha_{c_2} \approx 0.6$. For $\alpha < \alpha_{c_1}$ the ground-state (gs) phase exhibits Néel magnetic LRO, whereas for $\alpha > \alpha_{c_2}$ it exhibits collinear stripe-ordered LRO.

Send offprint requests to:

As already noted above, the spin quantum number s can, both in principle and in practice, play an important role in the phase structure of strongly correlated spin-lattice systems, which often display rich and interesting phase scenarios due to the interplay between the quantum fluctuations and the competing interactions. Varying the spin quantum number s can tune the strength of the quantum fluctuations and lead to fascinating phenomena [5]. A well-known example of such spin-dependent behaviour is the gapped Haldane phase [6] in $s = 1$ one-dimensional (1D) chains, which is not present in their $s = \frac{1}{2}$ counterparts.

Some recent studies on large-spin (i.e., $s > \frac{1}{2}$) systems include: (a) the comparison of the Heisenberg antiferromagnet (HAF) on the Sierpiński gasket with the corresponding HAFs on various regular 2D lattices, including the square, honeycomb, triangular and kagomé lattices, for the cases $s = \frac{1}{2}$, 1, and $\frac{3}{2}$ [7]; (b) the one-dimensional (1D) Heisenberg chain for both integral and half-odd integral values of s up to a value of 10 [8,9,10]; (c) the 2D J - J' model on the square lattice containing two different types of NN bonds, for values of s between $\frac{1}{2}$ and 2 [5]; (d) the 2D spin-anisotropic XXZ Heisenberg Hamiltonian for $s = 1$ [8,11,12,13]; (e) the spatially anisotropic J_1 - J_1' - J_2 model on the 2D square lattice for values of s up to 4 [14,15]; (f) the spin-anisotropic J_1^{XXZ} - J_2^{XXZ} model for $s = 1$ [16]; (g) the pure J_1 - J_2 model for $s = 1$ [17]; (h) the 2D Union Jack model for $s = 1$ and $s = \frac{3}{2}$ [18]; and the 2D Heisenberg model on the honeycomb lattice for $s = 1$ [19]. Another example that has been experimentally studied involves the investigation of the single-ion anisotropy energy in the 2D kagomé lattice for the case $s = \frac{5}{2}$ [20].

Also noteworthy in this context is the recent discovery of superconductivity with a transition temperature at $T_c \approx 26$ K in the layered iron-based compound LaOFeAs, when doped by partial substitution of the oxygen atoms by fluorine atoms [21]. This finding has been followed by the rapid discovery of superconductivity at even higher values of T_c ($\gtrsim 50$ K) in a broad class of similar quaternary compounds. Enormous interest has thereby been engendered in this class of materials. The very recent first-principles calculations [22] shows, for example, that the undoped parent precursor material LaOFeAs of the first material investigated in this oxypnictide class is well described by the spin-1 J_1 - J_2 model on the square lattice.

We have previously used the coupled cluster method (CCM) [23,24,25] to study the magnetic order in a spin-half interpolating square-triangle HAF (viz., the J_1 - J_2' model) [26,27]. This is a variant of the well-known J_1 - J_2 model on the infinite 2D square lattice, described below, in which one half of the NNN J_2 bonds are removed. In the present paper we further the investigation of the J_1 - J_2' model by replacing the spin- $\frac{1}{2}$ particles by particles with $s = 1$ and $s = \frac{3}{2}$. The 2D spin- $\frac{1}{2}$ J_1 - J_2' model has also been studied recently by other means [28,29,30,31], but we know of no other studies of the model for spins with spin quantum number $s > \frac{1}{2}$.

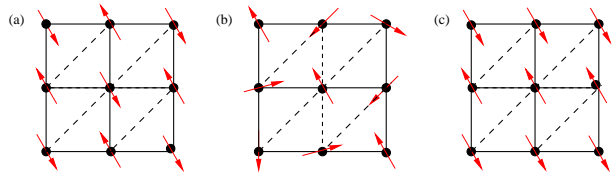


Fig. 1: (colour online) J_1 - J_2' model; $-J_1$; $---$ J_2' ; (a) Néel state, (b) spiral state, (c) striped state.

2 The model

The Hamiltonian of the J_1 - J_2' model is written as

$$H = J_1 \sum_{\langle i,j \rangle} \mathbf{s}_i \cdot \mathbf{s}_j + J_2' \sum_{[i,k]} \mathbf{s}_i \cdot \mathbf{s}_k \quad (1)$$

where the operators $\mathbf{s}_i \equiv (s_i^x, s_i^y, s_i^z)$ are the spin operators on lattice site i , with $\mathbf{s}_i^2 = s(s+1)$, and we consider here the cases $s = 1$ and $s = \frac{3}{2}$. On the square lattice the sum over $\langle i,j \rangle$ runs over all distinct NN bonds, but the sum over $[i,k]$ runs only over one half of the distinct NNN bonds with equivalent bonds chosen in each square plaquette, as shown explicitly in Fig. 1. We shall be interested here only in the case of competing (or frustrating) antiferromagnetic bonds $J_1 > 0$ and $J_2' > 0$, and henceforth for all of the results shown we set $J_1 \equiv 1$. Clearly, the model may be described equivalently as a Heisenberg model on an anisotropic triangular lattice in which each triangular plaquette contains two NN J_1 bonds and one NN J_2' bond. The model thus interpolates continuously between HAFs on a square lattice ($J_2' = 0$) and on a triangular lattice ($J_2' = J_1$). Similarly, when $J_1 = 0$ (or $J_2' \rightarrow \infty$ in our normalization with $J_1 \equiv 1$) the model reduces to uncoupled 1D chains (along the chosen diagonals on the square lattice). The case $J_2' \gg 1$ thus corresponds to weakly coupled 1D chains, and hence the model also interpolates between 1D and 2D scenarios. As well as the obvious theoretical richness of the model, there is also experimental interest since it is also believed to well describe such quasi-2D crystalline materials as organic compounds containing BEDT-TTF [32], for which with J_2'/J_1 lies typically in the range from about 0.3 to about 1; and Cs_2CuCl_4 [33], for which J_2'/J_1 takes a value of about 6, thus making this material even quasi-1D.

The J_1 - J_2' model has only two gs phases in the classical case (corresponding to the limit where the spin quantum number $s \rightarrow \infty$). For $J_2' < \frac{1}{2}J_1$ the gs phase is Néel ordered, as shown in Fig. 1(a), whereas for $J_2' > \frac{1}{2}J_1$ it has spiral order, as shown in Fig. 1(b), wherein the spin direction at lattice site (i,j) points at an angle $\alpha_{ij} = \alpha_0 + (i+j)\alpha_{\text{cl}}$, with $\alpha_{\text{cl}} = \cos^{-1}(-\frac{J_1}{2J_2'}) \equiv \pi - \phi_{\text{cl}}$. The pitch angle $\phi_{\text{cl}} = \cos^{-1}(\frac{J_1}{2J_2'})$ thus measures the deviation from Néel order, and it varies from zero for $2J_2'/J_1 \leq 1$ to $\frac{1}{2}\pi$ as $J_2'/J_1 \rightarrow \infty$, as shown later in Fig. 3. When $J_2' = J_1$ we regain the classical 3-sublattice ordering on the triangular lattice with $\alpha_{\text{cl}} = \frac{2}{3}\pi$. The classical phase transition at $J_2' = \frac{1}{2}J_1$ is of continuous (second-order) type, with the gs energy and its derivative both continuous.

In the limit of large J'_2/J_1 the above classical limit represents a set of decoupled 1D HAF chains (along the diagonals of the square lattice) with a relative spin orientation between neighboring chains that approaches 90° . In fact, of course, there is complete degeneracy at the classical level in this limit between all states for which the relative ordering directions of spins on different HAF chains are arbitrary. Clearly the exact spin- $\frac{1}{2}$ limit should also be a set of decoupled HAF chains as given by the exact Bethe ansatz solution [34]. However, one might expect that this degeneracy could be lifted by quantum fluctuations by the well-known phenomenon of *order by disorder* [35]. Just such a phase is known to exist in the J_1 - J_2 model [36, 37] for values of $J_2/J_1 \gtrsim 0.6$, where it is the so-called collinear striped phase in which, on the square lattice, spins along (say) the rows in Fig. 1 order ferromagnetically while spins along the columns and diagonals order antiferromagnetically, as shown in Fig. 1(c). We investigate the possibility below whether a stripe-ordered phase may be stabilized by quantum fluctuations at larger values of κ for either of the cases $s = 1$ or $s = \frac{3}{2}$, in order to compare with the earlier $s = \frac{1}{2}$ case for which we found [26] that such a gs phase might exist for high enough values of the frustration parameter κ , as discussed below.

Thus, for the $s = \frac{1}{2}$ case our own CCM calculations [26] provided strong evidence that the spiral phase becomes unstable at large values of the frustration parameter κ . In view of that observation we also used the CCM for the $s = \frac{1}{2}$ case with the collinear stripe-ordered state as a model state. We found tentative evidence, based on the relative energies of the two states, for a second zero-temperature phase transition between the spiral and stripe-ordered states at a larger critical value of $\kappa_{c_2} \approx 1.8 \pm 0.4$, as well as firm evidence for a first phase transition between the Néel antiferromagnetic phase and the helical phase at a critical coupling $\kappa_{c_1} = 0.80 \pm 0.01$.

The transition at $\kappa = \kappa_{c_1}$ for the $s = \frac{1}{2}$ case was found to be an interesting one. As in the classical ($s \rightarrow \infty$) case, the energy and its first derivative appeared to be continuous (within the errors inherent in our approximations), thus providing a typical scenario of a second-order phase transition, although a weakly first-order one could not be excluded since the gs energy did in fact show some definite signs of a (weak) discontinuity in slope. Furthermore, the average on-site magnetization was seen to approach a value $M_{c_1} = 0.025 \pm 0.025$ very close to zero on both sides of the transition, but with a very sharp drop and hence a possible discontinuity in M on the spiral side of the transition, as is often more typical of a first-order transition.

A particular interest here is to compare and contrast the corresponding transition(s) between the $s = \frac{1}{2}$ and the $s > \frac{1}{2}$ models. By contrast with the $s = \frac{1}{2}$ we shall find below that for the cases with $s = 1$ and $s = \frac{3}{2}$ the average on-site magnetization at the analogous phase transition between Néel-ordered and spirally-ordered states approaches smoothly the same nonzero value on both sides of the transition. Such continuous phase transitions where the order parameter does not vanish are well known in quantum magnetism. A prototypical example is the $s = \frac{1}{2}$

anisotropic XXZ model with a Hamiltonian given by

$$H = J \sum_{\langle i,j \rangle} (s_i^x s_j^x + s_i^y s_j^y + \Delta s_i^z s_j^z), \quad (2)$$

and which thus contains only NN anisotropic, antiferromagnetic ($J > 0$) Heisenberg bonds. Classically (corresponding to the $s \rightarrow \infty$ limit) the model has a continuous phase transition at $\Delta = \Delta_c \equiv 1$ between two different Néel antiferromagnetic phases, one aligned along the z -axis for $\Delta > 1$, and the other along some arbitrary direction in the perpendicular xy -plane for $-1 < \Delta < 1$. The $s = \frac{1}{2}$ model may also be solved exactly on a 1D chain by the Bethe ansatz technique [38]. It is found in this 1D case that as the critical point is approached, $\Delta \rightarrow \Delta_c = 1$, from either side, the average on-site (or staggered) magnetization $M \rightarrow M_c = 0$. The approach to zero is of a quite nontrivial kind, via a function with an essential singularity at $\Delta = \Delta_c$. By contrast, for the same $s = \frac{1}{2}$ XXZ model of Eq. (2) on a 2D square lattice, $M \rightarrow M_c \approx 0.31$ as $\Delta \rightarrow \Delta_c = 1$. Thus, the type of phase transition we observe below for the spin-1 and $s = \frac{3}{2}$ 2D interpolating square-triangle Heisenberg antiferromagnets is quite analogous to the one at $\Delta = \Delta_c = 1$ in the $s = \frac{1}{2}$ XXZ model on the 2D square lattice, but not to that of the same XXZ model on the 1D chain.

We now first briefly describe the main elements of the CCM below in Sec. 3, where we also discuss the approximation schemes used in practice for the $s = \frac{1}{2}$ case and the $s > \frac{1}{2}$ cases. Then in Sec. 4 we present our CCM results based on using the Néel, spiral and striped states discussed above as model states (or starting states). We conclude in Sec. 5 with a discussion of the results.

3 The coupled cluster method

The CCM (see, e.g., Refs. [23, 24, 25] and references cited therein) is regarded as one of the most powerful and most versatile modern techniques in quantum many-body theory. It has been successfully applied to many quantum magnets (see Refs. [4, 25, 36, 37, 39, 40, 41, 42, 43, 44]) and references cited therein). The CCM is suitable for studying frustrated systems, for which the main alternative methods are often only of limited usefulness. For example, quantum Monte Carlo techniques are usually restricted by the sign problem for such systems, and the exact diagonalization method is limited in practice, especially for $s > \frac{1}{2}$, to such small lattices that it is often insensitive to the details of any subtle phase order present.

The CCM method to solve the gs Schrödinger ket and bra equations, $H|\Psi\rangle = E|\Psi\rangle$ and $\langle\tilde{\Psi}|H = E\langle\tilde{\Psi}|$ respectively is now briefly outlined (and see Refs. [9, 23, 24, 25, 39, 40] for further details). The implementation of the CCM is initiated by the selection of a model state $|\Phi\rangle$ on top of which to incorporate later in a systematic fashion the multispin correlations contained in the exact ground states $|\Psi\rangle$ and $\langle\tilde{\Psi}|$. The CCM employs the exponential ansatz, $|\Psi\rangle = e^S|\Phi\rangle$ and $\langle\tilde{\Psi}| = \langle\Phi|\tilde{S}e^{-S}$. The creation correlation operator S is written as $S = \sum_{I \neq 0} S_I C_I^+$ with its

destruction counterpart as $\tilde{S} = 1 + \sum_{I \neq 0} \tilde{S}_I C_I^-$. The operators $C_I^+ \equiv (C_I^-)^\dagger$, with $C_0^+ \equiv 1$, have the property that $\langle \Phi | C_I^+ = 0 = C_0^- | \Phi \rangle; \forall I \neq 0$. They form a complete set of multispin creation operators with respect to the model state $|\Phi\rangle$. The calculation of the ket- and bra-state correlation coefficients $(\mathcal{S}_I, \tilde{\mathcal{S}}_I)$ is performed by requiring the gs energy expectation value $\tilde{H} \equiv \langle \tilde{\Psi} | H | \tilde{\Psi} \rangle$ to be a minimum with respect to each of them. This results in a coupled set of equations $\langle \Phi | C_I^- e^{-S} H e^S | \Phi \rangle = 0$ and $\langle \Phi | \tilde{S} (e^{-S} H e^S - E) C_I^+ | \Phi \rangle = 0; \forall I \neq 0$, which we normally solve by using parallel computing routines [45] for the correlation coefficients $(\mathcal{S}_I, \tilde{\mathcal{S}}_I)$ within specific truncation schemes as outlined below.

In order to treat each lattice site on an equal footing a mathematical rotation of the local spin axes on each lattice site is performed such that every spin of the model state aligns along its negative z -axis. As a result, our description of the spins is given wholly in terms of these locally defined spin coordinate frames. The multispin creation operators may be expressed as $C_I^+ \equiv s_{i_1}^+ s_{i_2}^+ \cdots s_{i_n}^+$, in terms of the locally defined spin-raising operators $s_i^+ \equiv s_i^x + s_i^y$ on lattice sites i . Upon solving for the multispin cluster correlation coefficients $(\mathcal{S}_I, \tilde{\mathcal{S}}_I)$ as outlined above, the gs energy E may then be calculated from the relation $E = \langle \Phi | e^{-S} H e^S | \Phi \rangle$, and the gs staggered magnetization M from the relation $M \equiv -\frac{1}{N} \langle \tilde{\Psi} | \sum_{i=1}^N s_i^z | \tilde{\Psi} \rangle$ in terms of the rotated spin coordinates.

If a complete set of multispin configurations $\{I\}$ with respect to the model state $|\Phi\rangle$ is included in the calculation of the correlation operators S and \tilde{S} , then the CCM formalism becomes exact. However, it is necessary in practical applications to use systematic approximation schemes to truncate them to some finite subset. For the $s = \frac{1}{2}$ case, the localised LSUB n scheme is commonly employed, as in our earlier paper on the $s = \frac{1}{2}$ version of the present model [26], as well as in our other previous work [9, 25, 39, 40, 43]. Under this truncation scheme all possible multi-spin-flip correlations over different locales on the lattice defined by n or fewer contiguous lattice sites are retained. A cluster is defined as having n contiguous sites if every one of the n sites is adjacent (as a nearest neighbour) to at least one other. Clearly this definition, however, depends on how we choose the geometry of the lattice among various topologically equivalent possibilities that may exist. For example, the current model may be construed as referring to sites on a square lattice, as shown in Fig. 1. In this case the J_2' bonds, for example, join NNN sites (which, by definition, are thus not adjacent). Alternatively, the model may be equivalently construed as referring to sites on a triangular lattice, in which case both J_1 and J_2' bonds join NN (and hence adjacent) sites. In all of the results presented here we consider the model to be defined on a triangular lattice in making CCM approximations.

However, we note that the number of fundamental LSUB n configurations for $s > \frac{1}{2}$ becomes appreciably higher than for $s = \frac{1}{2}$, since each spin on each site i can now be raised up to $2s$ times by the spin-raising operator s_i^+ . Thus, for the $s > \frac{1}{2}$ models it is more practi-

Table 1: Number of fundamental CCM configurations (N_f) for the SUB n - n ($n = \{2, 3, 4, 5, 6, 7\}$) scheme for the Néel and striped model states, for the J_1 - J_2' model defined on a triangular lattice, for the spin-1 and spin- $\frac{3}{2}$ cases.

Method	$s = 1$		$s = \frac{3}{2}$	
	N_f		N_f	
SUB n - n	striped	spiral	striped	spiral
SUB2-2	2	4	2	4
SUB3-3	4	26	4	27
SUB4-4	60	189	60	211
SUB5-5	175	1578	175	1908
SUB6-6	2996	14084	3622	18501
SUB7-7	11778	131473	13320	188326

cal, but equally systematic, to use the alternative SUB n - m scheme, in which all correlations involving up to n spin flips spanning a range of no more than m contiguous lattice sites are retained [15, 16, 18, 25, 41]. We then set $m = n$, and hence employ the so-called SUB n - n scheme. More generally, the LSUB m scheme is thus equivalent to the SUB n - m scheme for $n = 2sm$ for particles of spin s . For $s = \frac{1}{2}$, LSUB $n \equiv$ SUB n - n ; whereas for $s > \frac{1}{2}$, LSUB $n \equiv$ SUB $2sn$ - n . The numbers of such fundamental configurations (viz., those that are distinct under the symmetries of the Hamiltonian and of the model state $|\Phi\rangle$) that are retained for the Néel and striped model states of the current $s = 1$ and $s = \frac{3}{2}$ models at various SUB n - n levels, defined with respect to an underlying triangular-lattice geometry, are shown in Table 1.

Although we never need to perform any finite-size scaling, since all CCM approximations are automatically performed from the outset in the $N \rightarrow \infty$ limit, where N is the total number of lattice sites, we do need as a last step to extrapolate to the $n \rightarrow \infty$ limit in the truncation index n . We use here the well-tested [15, 16, 26, 40, 41] empirical scaling laws

$$E/N = a_0 + a_1 n^{-2} + a_2 n^{-4}, \quad (3)$$

$$M = b_0 + b_1 n^{-1} + b_2 n^{-2}, \quad (4)$$

exactly as we did previously for the corresponding $s = \frac{1}{2}$ model [26], for the gs energy per spin E/N and the gs staggered magnetization M , respectively.

4 Results

The results of the CCM calculations are reported here for the spin-1 and spin- $\frac{3}{2}$ J_1 - J_2' model Hamiltonian of Eq. (1), using the Néel, spiral and striped states shown in Fig. 1(a)-(c) as CCM model states, and with the SUB n - n approximation scheme defined with respect to an underlying triangular-lattice geometry. We set the parameter $J_1 = 1$. Our available computational power at present is such that we can perform SUB n - n calculations for the spiral model

state (viz., the state that requires the highest number of fundamental configurations (N_f) for a given SUB n - n truncation index n) only for values $n \leq 7$ for both the $s = 1$ and $s = \frac{3}{2}$ cases. We thus present results for each of the Néel, striped and spiral states only up to the SUB7-7 level, for the sake of consistency in our extrapolations to the $n \rightarrow \infty$ limit.

We note that, as has been well documented in the past [46], the LSUB n (or SUB n - n) data for both the gs energy per spin E/N and the average on-site magnetization M converge differently for even- n sequences and odd- n sequences, similar to what is frequently observed in perturbation theory [47]. Since, as a general rule, it is desirable to have at least $(n + 1)$ data points to fit to any fitting formula that contains n unknown parameters, we prefer to have at least 4 results to fit to Eqs. (3) and (4). Both the available odd and even series of our SUB n - n data violate this desirable rule. However, our results (for both sets $n = \{2, 4, 6\}$ and $n = \{3, 5, 7\}$) for the $s = \frac{1}{2}$ case are consistent with those using the larger LSUB m sequences available in this case. This gives us confidence in both the accuracy of our results and the robustness of our extrapolation schemes. Hence, for most of our extrapolated results below we use the even SUB n - n sequence with $n = \{2, 4, 6\}$ and the odd SUB n - n sequence with $n = \{3, 5, 7\}$.

Firstly, the results obtained using the spiral model state are reported. For this state we first perform CCM calculations with the pitch angle ϕ as a free parameter. At each separate level of approximation we then choose the angle $\phi = \phi_{\text{SUB}n-n}$ that minimizes the energy $E_{\text{SUB}n-n}(\phi)$.

Classically we have a second-order phase transition from Néel order (for $\kappa < \kappa_{\text{cl}}$) to helical order (for $\kappa > \kappa_{\text{cl}}$), where $\kappa \equiv J_2/J_1$, at a value $\kappa_{\text{cl}} = 0.5$. By contrast, our CCM results presented below show that there is a shift of this critical point to a value $\kappa_c \approx 0.615 \pm 0.010$ in the spin-1 quantum case and $\kappa_c \approx 0.575 \pm 0.005$ for the spin- $\frac{3}{2}$ quantum case, first indications of which are seen in Figs. 2 and 3. In both cases this is a second-order phase transition from Néel-ordered to helically-ordered states. Thus, for example, curves such as those shown in Fig. 2 show that the Néel state ($\phi = 0$) gives the minimum gs energy for all values of $\kappa < \kappa_c$, where κ_c depends on the level of SUB n - n approximation used, as we also observe in Fig. 3. By contrast, for values of $\kappa > \kappa_c$ the minimum in the energy is found to occur at a value $\phi \neq 0$. If we consider the pitch angle ϕ itself as an order parameter (i.e., $\phi = 0$ for Néel order and $\phi \neq 0$ for spiral order) a typical scenario for a phase transition would be the appearance of a two-minimum structure for the gs energy for values of $\kappa > \kappa_c$, exactly as observed in Fig. 2 for both the spin-1 and spin- $\frac{3}{2}$ models in the SUB4-4 approximation. Very similar curves occur for other SUB n - n approximations.

We note that the crossover from one minimum ($\phi = 0$, Néel) solution to the other ($\phi \neq 0$, spiral) appears to be quite smooth at this point (and see Figs. 2 and 3). Thus, for example, the spiral pitch angle ϕ appears to change quite continuously from a value of zero for $\kappa < \kappa_c$ on the Néel side of the transition to a nonzero value for $\kappa > \kappa_c$ on the spiral-phase side. For example, at the SUB6-6 level

we find $\kappa_c \approx 0.613$ for the spin-1 case, and $\kappa_c \approx 0.574$ for the spin-spin- $\frac{3}{2}$ case. We also note from Fig. 3 that as $J_2 \rightarrow \infty$ the spiral angle ϕ approaches the limiting value $\frac{1}{2}\pi$ considerably slower for the spin-1 and spin- $\frac{3}{2}$ cases than it does the spin- $\frac{1}{2}$ case we investigated earlier (and see Fig. 3 in Ref. [26]). This is a first indication that there is less freedom for the existence of a stable collinear (striped) state at higher values of κ for the higher spin ($s > \frac{1}{2}$) models than for the $s = \frac{1}{2}$ model. We return to this point later.

Figure 2 shows the ground-state energy per spin versus the spiral angle ϕ , using the SUB4-4 approximation of the CCM with the spiral model state, for some illustrative values of J_2 . Similarly Fig. 3 shows the angle $\phi_{\text{SUB}n-n}$ that minimizes the energy $E_{\text{SUB}n-n}(\phi)$. Our previous study of the quantum spin- $\frac{1}{2}$ case in the same model [26] found that there is a first quantum critical point at $\kappa_{\text{cl}} \approx 0.80$ at which a weakly first-order, or possibly second-order, phase transition occurs between states that exhibit Néel order and helical order. We see now that increasing the spin quantum number s thus brings the quantum critical point κ_c closer to the classical critical point $\kappa_{\text{cl}} = 0.5$ for the phase transition from Néel order to helical order, as expected.

We observe from Fig. 2 that for certain values of J_2' (or, equivalently, κ) CCM solutions at a given SUB n - n level of approximation (viz., SUB4-4 in Fig. 2) exist only for certain ranges of the spiral angle ϕ . For example, for the pure square-lattice HAF ($\kappa = 0$) the CCM SUB4-4 solution based on a spiral model state only exists for $0 \leq \phi \lesssim 0.17\pi$ for the spin-1 model and $0 \leq \phi \lesssim 0.16\pi$ for the spin- $\frac{3}{2}$ model. In this case, where the Néel solution is the stable ground state, if we attempt to move too far away from Néel collinearity the CCM equations themselves become “unstable” and simply do not have a real solution. Similarly, we see from Fig. 2 that for $\kappa = 1.5$ the CCM SUB4-4 solution exists only for $0.25\pi \lesssim \phi \leq 0.5\pi$ for the spin-1 model and for $0.27\pi \lesssim \phi \leq 0.5\pi$ for the spin- $\frac{3}{2}$ model. In this case the stable ground state is a spiral phase, and now if we attempt to move too close to Néel collinearity the real solution terminates.

Such terminations of CCM solutions are common [25]. A termination point usually arises because the solutions to the CCM equations become complex at this point, beyond which there exist two branches of entirely unphysical complex conjugate solutions [25]. In the region where the solution reflecting the true physical solution is real there actually also exists another (unstable) real solution. However, only the (shown) upper branch of these two solutions reflects the true (stable) physical ground state, whereas the lower branch does not. The physical branch is usually easily identified in practice as the one which becomes exact in some known (e.g., perturbative) limit. This physical branch then meets (with infinite slope, as seen in Fig. 2) the corresponding unphysical branch at some termination point beyond which no real solutions exist. The SUB n - n termination points are themselves also reflections of the quantum phase transitions in the real system, and may be used to estimate the position of the phase boundary

[25], although we do not do so here since we have more accurate criteria discussed below.

Figures 4 and 5 show the CCM results for the gs energy and average gs on-site magnetization, respectively, where the spiral state has been used as the model state. The gs energy (in Fig. 4) shows no sign of a discontinuity in slope at the critical values κ_c discussed above, and this is an indication of a second-order transition from the Néel phase to the helical phase. This is in contrast with the spin- $\frac{1}{2}$ case, where the gs energy shows definite signs of a (weak) discontinuity in slope at the first critical value κ_{c_1} [26].

The gs magnetic order parameter M in Fig. 5 shows much clearer evidence of a phase transition at the corresponding κ_c values previously observed in Fig. 3. Thus, we see that for the spin-1 case the sharp minimum in the extrapolated magnetic order parameter occurs at $\kappa_c \approx 0.613$ (with $M_c = 0.6367$) using $n = \{2, 4, 6\}$ for the extrapolation of M , and at $\kappa_c \approx 0.606$ (with $M_c = 0.5978$) using $n = \{3, 5, 7\}$; whereas for the spin- $\frac{3}{2}$ case, the corresponding values are $\kappa_c \approx 0.574$ (with $M_c = 1.1134$) using $n = \{2, 4, 6\}$ for the extrapolation of M and at $\kappa_c \approx 0.571$ (with $M_c = 1.0766$) using $n = \{3, 5, 7\}$. We also present other independent estimates for κ_c below.

By contrast, for the spin- $\frac{1}{2}$ case [26] the extrapolated value of M showed clearly its steep drop toward a value very close to zero at a corresponding value $\kappa_c \approx 0.80$, which gave the best CCM estimate of the phase-transition point for that case. In the spin- $\frac{1}{2}$ case the magnetization seemed to approach continuously a value $M = 0.025 \pm 0.025$ from the Néel side ($\kappa < \kappa_c$) whereas from the spiral side ($\kappa > \kappa_c$) there appeared to be a discontinuous jump in M as $\kappa \rightarrow \kappa_c$. The transition at $\kappa < \kappa_c$ thus appeared to be (very) weakly first order but it was not possible to exclude it being second order since the possibility of a continuous but very steep drop to zero of the on-site magnetization as $\kappa \rightarrow \kappa_c$ from the spiral side of the transition could not be entirely ruled out. No evidence at all was found for any intermediate phase between the quasiclassical Néel and spiral phases, just as for the higher-spin cases considered here. However, Fig. 5 here shows no evidence at all for a finite jump in M as $\kappa \rightarrow \kappa_c$ from either side of the transition, and hence the evidence from the order parameter is that the transition from Néel order to spiral order for both the spin-1 and spin- $\frac{3}{2}$ cases is of second-order type.

Table 2 shows the critical values $\kappa_c^{\text{SUB}n-n}$ at which the transition between the Néel and spiral phases occurs in the various SUB n - n approximations shown in Fig. 3. In the past we have found that a simple linear extrapolation scheme [4, 18, 44], $\kappa_c^{\text{SUB}n-n} = a_0 + a_1 n^{-1}$, yields a good fit to such critical points. This seems to be the case here too, just as for the spin- $\frac{1}{2}$ case [26]. The fact that the two corresponding ‘‘SUB ∞ ’’ estimates from the SUB n - n data in Table 2 based on the even- n and odd- n SUB n - n sequences differ slightly from one another is a reflection of the errors inherent in our extrapolation procedures. Similar estimates based on an alternative extrapolation scheme, $\kappa_c^{\text{LSUB}n} = b_0 + b_1 n^{-2}$, are also shown in

Table 2: The critical value $\kappa_c = \kappa_c^{\text{SUB}n-n}$ at which the transition between the Néel phase ($\phi = 0$) and the spiral phase ($\phi \neq 0$) occurs in various SUB n - n approximations, using the CCM with the (Néel or) spiral state as model state, for the J_1 - J'_2 model. Results are shown for both the spin-1 and spin- $\frac{3}{2}$ cases.

Method	$s = 1$	$s = \frac{3}{2}$
	κ_c	κ_c
SUB2-2	0.597	0.563
SUB4-4	0.610	0.571
SUB6-6	0.613	0.574
SUB ∞^a	0.617	0.581
SUB ∞^b	0.616	0.577
SUB3-3	0.577	0.554
SUB5-5	0.597	0.566
SUB7-7	0.607	0.571
SUB ∞^c	0.636	0.583
SUB ∞^d	0.619	0.577

^a Based on $1/n : n = \{2, 4, 6\}$
^b Based on $1/n^2 : n = \{2, 4, 6\}$
^c Based on $1/n : n = \{3, 5, 7\}$
^d Based on $1/n^2 : n = \{3, 5, 7\}$

Table 2. The difference between all of these estimates is thus also a rough indication of our real error bars on κ_c .

It is gratifying to note that all of the estimates for κ_c from the extrapolations of our computed results for $\kappa_c^{\text{SUB}n-n}$ are in excellent agreement with those obtained from the extrapolated results for the order parameter M discussed above. By putting all of these results together, our final estimates for the critical point for the transition between the Néel-ordered and the spirally-ordered phases are $\kappa_c = 0.615 \pm 0.010$ for the spin-1 model and $\kappa_c = 0.575 \pm 0.005$ for the spin- $\frac{3}{2}$ model.

We conclude our discussion of the Néel and spiral phases by presenting detailed results for the two spin cases for the two special limits of the model, namely the pure isotropic HAF on the square and triangular lattices. Thus, Table 3 shows the results for the ground-state energy per spin and magnetic order parameter (i.e., the average on-site magnetization) for the spin-1 and spin- $\frac{3}{2}$ J_1 - J'_2 HAF model on the square lattice ($J'_2 = 0$ or $\kappa = 0$) and on the triangular lattice ($J'_2 = J_1$ or $\kappa = 1$), using the spiral model state. Our CCM results are presented in various SUB n - n approximations (with $2 \leq n \leq 7$) based on the triangular lattice geometry using the spiral model state, with $\phi = 0$ for the square lattice and $\phi = \frac{\pi}{3}$ for the triangular lattice. The extrapolated results ($n \rightarrow \infty$) using Eqs. (3) and (4) with $n = \{2, 4, 6\}$ and $n = \{3, 5, 7\}$ are also presented. For comparison we also show the results obtained for the spin-1 model on the square lattice (i.e., $\kappa = 0$) using spin-wave theory (SWT) [48], a linked-cluster series expansion (SE) method [49], and previous CCM SUB n - n ($n \rightarrow \infty$) results based on the model construed as referring to sites on a square lattice [13]. Our present results are seen both to

Table 3: Ground-state energy per spin and magnetic order parameter (i.e., the average on-site magnetization) for the spin-1 and spin- $\frac{3}{2}$ HAFs on the square and triangular lattices. We show CCM results obtained for the J_1 - J'_2 model with $J_1 > 0$, using the spiral model state in various SUB n - n approximations defined on the triangular lattice geometry, for the two cases $\kappa \equiv J'_2/J_1 = 0$ (square lattice HAF, $\phi = 0$) and $\kappa = 1$ (triangular lattice HAF, $\phi = \frac{\pi}{3}$).

Method	$s = 1$				$s = \frac{3}{2}$			
	E/N		M		E/N		M	
	square ($\kappa = 0$)		triangular ($\kappa = 1$)		square ($\kappa = 0$)		triangular ($\kappa = 1$)	
SUB2-2	-2.29504	0.9100	-1.77400	0.9069	-4.94393	1.4043	-3.80006	1.3938
SUB3-3	-2.29763	0.9059	-1.80101	0.8791	-4.94836	1.3990	-3.83393	1.3672
SUB4-4	-2.31998	0.8702	-1.82231	0.8405	-4.97694	1.3638	-3.86025	1.3287
SUB5-5	-2.32049	0.8682	-1.82623	0.8294	-4.97789	1.3611	-3.86498	1.3170
SUB6-6	-2.32507	0.8510	-1.83135	0.8096	-4.98305	1.3452	-3.87059	1.2980
SUB7-7	-2.32535	0.8492	-1.83288	0.8006	-4.98344	1.3430	-3.87191	1.2904
Extrapolations								
SUB ∞ ^a	-2.32924	0.8038	-1.83860	0.7345	-4.98793	1.3001	-3.87869	1.2233
SUB ∞ ^b	-2.32975	0.7938	-1.83968	0.7086	-4.98803	1.2933	-3.87839	1.2107
CCM ^c	-2.3291	0.8067						
SWT ^d	-2.3282	0.8043						
SE ^e	-2.3279(2)	0.8039(4)						

^a Based on $n = \{2, 4, 6\}$

^b Based on $n = \{3, 5, 7\}$

^c CCM (SUB ∞ for square lattice, based on $n = \{2, 4, 6\}$) in the natural square-lattice geometry [13]

^d SWT (Spin-wave theory) for square lattice [48]

^e SE (Series Expansion) for square lattice [49]

be robust and internally consistent, by comparison of the independent extrapolations of the SUB n - n data using the even- n and odd- n data sets, and to agree very well with the best alternative results available for the spin-1 model on the square lattice. Such comparisons give us confidence that our results are likely to be similarly accurate over the entire range of values of the frustration parameter κ .

We turn finally to our CCM results based on the collinear striped AFM state as the choice for the CCM gs model state $|\Phi\rangle$. The SUB n - n configurations are again defined with respect to the triangular lattice geometry, exactly as before. The numbers of fundamental configuration N_f in each of the SUB n - n approximations used are given in Table 1. Results for the gs energy and magnetic order parameter based on the striped phase are shown in Figs. 6 and 7 respectively. We see from Fig. 6 that some of the SUB n - n solutions based on the striped state for both the $s = 1$ and $s = \frac{3}{2}$ cases show a clear termination point κ_t of the sort discussed previously, such that for $\kappa < \kappa_t$ no real solution for the striped phase exists.

For the spin-1 model the large- κ limit of the extrapolated SUB n - n energy per spin results of $E/N = -1.3897J'_2$ from Fig. 6(a) using $n = \{2, 4, 6\}$ and $E/N = -1.3936J'_2$ from Fig. 6(b) using $n = \{3, 5, 7\}$ agree well with the known 1D chain result of $E/N = -1.4015$ obtained from a density-matrix renormalization group analysis [50] and our previous CCM result [9], just as in Fig. 4(a) and (b) for the spiral phase. Similarly, for the spin- $\frac{3}{2}$ case, the large- κ limit of the extrapolated SUB n - n results for the

energy per spin of $E/N = -2.8205J'_2$ from Fig. 6(c) using $n = \{2, 4, 6\}$ and $E/N = -2.8243J'_2$ from Fig. 6(d) using $n = \{3, 5, 7\}$, with almost identical results again obtained from Fig. 4(c) and (d). Unlike for their spin- $\frac{1}{2}$ counterpart, however, the striped phase is never a stable gs state for either the spin-1 or spin- $\frac{3}{2}$ models, because their energies always lie higher than those of the spiral state for all values of J'_2 , as shown in Fig. 8. Hence for the $s = 1$ and $s = \frac{3}{2}$ cases, there is only one quantum critical point κ_c , at which the Néel phase is driven to the helical phase.

5 Discussion and conclusions

In an earlier paper [26] we used the CCM to study the effect of quantum fluctuations on the zero-temperature gs phase diagram of a frustrated spin- $\frac{1}{2}$ interpolating square-triangle antiferromagnetic model. This is the so-called J_1 - J'_2 model, defined on an anisotropic 2D lattice, as shown in Fig. 1. In the current paper we have extended the analysis to consider spin-1 and spin- $\frac{3}{2}$ versions of the same model. As before we have studied the case where the NN J_1 bonds are antiferromagnetic ($J_1 > 0$) and the competing $J'_2 \equiv \kappa J_1$ bonds have a strength κ that varies from $\kappa = 0$ (corresponding to the HAF on the square lattice) to $\kappa \rightarrow \infty$ (corresponding to a set of decoupled 1D HAF chains), with the HAF on the triangular lattice as another special case, $\kappa = 1$, in between the two extremes. The results of the $\kappa = 0$ limit of the present model (and see

Table 3) for the $s = 1$ case are comparable with those obtained from the SWT and SE techniques [48, 49] which are among the best alternative numerical method to the CCM for highly frustrated spin-lattice models like the present J_1 - J_2 model.

For the spin-1 model we find that the phase transition between the Néel antiferromagnetic phase and the spiral phase occurs at the value $\kappa_c = 0.615 \pm 0.010$, whereas for the spin- $\frac{3}{2}$ model we find that the phase transition occurs at $\kappa_c = 0.575 \pm 0.005$. From the continuous and smooth behaviour of the energies of the two phases it appears that the transition is second-order, as in the classical case. However, on neither side of the transition at κ_c does the order parameter M (i.e., the average on-site magnetization) go to zero for either of the two higher spins considered here. On the other hand, unlike in the spin- $\frac{1}{2}$ case, in neither of the higher-spin models does there appear to be any discontinuity in M at the transition. All of the indications are thus that the transition between the Néel antiferromagnetic and the spiral phases is of continuous (second-order) type for both cases $s = 1$ and $s = \frac{3}{2}$, in contrast to the spin- $\frac{1}{2}$ case where the order parameter M appeared to show a discontinuous jump at the transition, which was found to be a weakly first-order one (although it could not be entirely excluded on the available evidence that the transition might be a second-order one).

We have observed that as the quantum spin number s is increased, the position of the quantum critical point at κ_c between the phases with Néel and spiral order is brought closer to the classical ($s \rightarrow \infty$) value, $\kappa_{cl} = 0.5$, as expected. In contrast with the $s = \frac{1}{2}$ case where there is a second quantum critical point for the phase transition from the helical phase to a collinear stripe-ordered phase, we find no evidence at all for such a further transition for either of the cases $s = 1$ or $s = \frac{3}{2}$.

We note that the spin-1 HAF on the (undistorted) triangular lattice (viz., our limiting case $\kappa = 1$) has itself been the subject of much recent interest from both the theoretical and experimental viewpoints. From the experimental side spin-1 models on the triangular lattice are believed to underlie the properties of such materials as NiGa_2S_4 [51] and $\text{Ba}_3\text{NiSb}_2\text{O}_9$ [52]. In both materials the Ni^{2+} ions form in weakly coupled 2D triangular lattice layers. Thus, for example, thermodynamic and neutron scattering measurements on NiGa_2S_4 show conclusive evidence that the inherent geometric frustration of the triangular lattice stabilises a low-temperature spin-disordered state, which was proposed as being consistent with a spin-liquid phase [51]. Other candidates for spin-1 quantum spin-liquid phases have more recently been proposed from an experimental study of the high-pressure sequence of structural phases in the material $\text{Ba}_3\text{NiSb}_2\text{O}_9$ [52].

Whereas quantum fluctuations are certainly intrinsically greatest for spin-lattice systems with the lowest spin value $s = \frac{1}{2}$, as we have also found here, such effects can also be enhanced for the $s > \frac{1}{2}$ cases by the addition to the pure (bilinear) Heisenberg interaction with NN terms only of terms such as a NN biquadratic interaction or other higher-order exchange terms. It is precisely by the

addition of terms like this that unusual quantum ground states, such as ones with quadrupolar (or spin-nematic) order have been predicted theoretically to be stabilised for the spin-1 HAF on the triangular lattice [53, 54, 55, 56]. It is argued that such a state can account for the observed low-temperature thermodynamics in the spin-1, quasi-2D, antiferromagnetic material NiGa_2S_4 , although at the lowest temperatures the observed order is that of an (incommensurate) spiral phase. In a very recent paper (that appeared only after submission of this paper) [57] it is also argued that the quantum spin-liquid phases presumed to have been seen in recent experiments [52] in the layered material $\text{Ba}_3\text{NiSb}_2\text{O}_9$, may be explained microscopically as emanating from a spin-1 HAF on the triangular lattice with both NN and NNN isotropic antiferromagnetic Heisenberg couplings.

Such other (e.g., spin-1) models on the triangular lattice as those described above, involving either isotropic bilinear and biquadratic couplings or both NN and NNN bilinear Heisenberg couplings, could also be investigated via the CCM, and it would surely be interesting to do so. While such additional terms in the Hamiltonian present no additional obstacles to the use of the method at all, the choice of which model states to use always enters at the outset. It is certainly true that most calculations on spin systems employing the CCM, including those in the present paper, employ model states built by independent-spin product states for which the choice of state for the spin on each site is formally independent of the choice of all others. Often for these independent-spin product model states the use of collinear states, such as the Néel or striped states considered here, is possible, where all spins are aligned parallel or antiparallel to one axis. However, as we have seen, noncollinear (e.g. spiral) model states can sometimes be favourable for certain values of the frustration. In either case multispin correlations are then included systematically on top of the independent-spin product model states. As we have seen here, the CCM for such independent-spin product model states may then be applied to high orders by using a computational implementation used here and described more fully elsewhere (see, e.g., Refs. [39, 9, 45] and references cited therein). In particular, it may be applied to lattices of complex crystallographic symmetry. Furthermore, as seen here, it is not constrained to systems with spin quantum number $s = \frac{1}{2}$.

When the system under consideration may have more exotic ground states with less conventional ordering than the (often essentially quasiclassical) independent-spin product states described above, the CCM may still be very profitably employed. Even the use of such independent-spin product states can still give very precise phase boundaries for when such states give way to more exotic states. A good example among many to date is the well-studied frustrated spin- $\frac{1}{2}$ J_1 - J_2 model on the square lattice discussed in Sec. 1, for which the phase boundaries of the non-classical paramagnetic state (that has no magnetic LRO) have been estimated very accurately using the CCM in Refs. [36, 37]. A more recent example is provided by a CCM calculation [58] of the frustrated spin- $\frac{1}{2}$ J_1 - J_2 - J_3

model on the honeycomb lattice which incorporates NN bonds (J_1) and NNN bonds (J_2) as in the J_1 - J_2 model, but now also includes next-next-nearest-neighbour bonds (J_3). For the case $J_3 = J_2$ an intermediate paramagnetic phase was accurately located between collinear antiferromagnetic states of quasiclassical Néel and striped order. By calculating with such model states the plaquette susceptibility, the authors gave precise values not only of the phase boundaries of this intermediate state, but also gave clear evidence that it had plaquette valence-bond crystalline ordering.

It is also worth noting that the CCM can deal directly with more complex model states, such as those involving valence-bond crystal (VBC) order. Thus, for example, non-classical VBC ordering has been considered using the CCM by employing directly valence-bond model states, i.e. two- or multi-spin singlet product states [59]. A drawback of this approach is that it involves the direct use of products of localized states (e.g., two-spin dimers or multi-spin plaquettes) in the model state. Hence, this approach requires that a new matrix-operator formalism be created for each new problem. Also, the Hamiltonian and CCM ket- and bra-state operators must be written in terms of this new matrix algebra. The CCM equations may be derived and solved once the commutation relationships between the operators have been established. Although formally straightforward, this process can be tedious and time-consuming. Furthermore, the existing high-order CCM formalism and codes also need to be amended extensively for each separate model considered.

More recently a quite different CCM approach has been advocated for dealing with such VBC states [60]. It starts directly from collinear independent-spin product model states, and shows how one may form exact local dimer or plaquette ground states within the CCM framework. This approach has the huge advantages of being conceptually simple and thus also of being easy to implement. Furthermore, one may then use directly the existing high-order CCM formalism, computer codes, and extrapolation schemes used and described here and in that references cited. To date the method has been applied with excellent results to the spin- $\frac{1}{2}$ J_1 - J_2 model for the linear chain, the spin- $\frac{1}{2}$ Shastry-Sutherland model on the 2D square lattice [61], and the so-called spin- $\frac{1}{2}$ J - J' HAF on the 2D CAVO lattice that is appropriate to the magnetic material CaV_4O_9 . It is a one-fifth depleted square lattice, and the model on this lattice comprises two nonequivalent antiferromagnetic NN bonds of strength J and J' . The J bonds connect sites on the NN four-spin square plaquettes while the J' (dimer) bonds connect NN sites belonging to neighbouring square plaquettes.

In conclusion, it will be of interest to use the CCM for the other spin-1 models discussed above on the triangular lattice that are believed to be relevant to such quasi-2D materials as NiGa_2S_4 and $\text{Ba}_3\text{NiSb}_2\text{O}_9$, for both of which considerable experimental data exist. We hope to be able to perform and report ourselves on such calculations at a later date.

Acknowledgment

We thank the University of Minnesota Supercomputing Institute for Digital Simulation and Advanced Computation for the grant of supercomputing facilities, on which we relied heavily for the numerical calculations reported here. We also thank D. J. J. Farnell and C. E. Campbell for their assistance.

References

1. S. Sachdev, in *Low Dimensional Quantum Field Theories for Condensed Matter Physicists*, edited by Y. Lu, S. Lundqvist, and G. Morandi (World Scientific, Singapore 1995).
2. J. Richter, J. Schulenburg, and A. Honecker, in *Quantum Magnetism*, Lecture Notes in Physics **645**, edited by U. Schollwöck, J. Richter, D. J. J. Farnell, and R. F. Bishop (Springer-Verlag, Berlin, 2004), p. 85.
3. G. Misguich and C. Lhuillier, in *Frustrated Spin Systems*, edited by H. T. Diep (World Scientific, Singapore, 2005), p. 229.
4. R. F. Bishop, P. H. Y. Li, D. J. J. Farnell, and C. E. Campbell, Phys. Rev. B **82**, 024416 (2010).
5. R. Darradi, J. Richter, and D. J. J. Farnell, J. Phys.: Condens. Matter, **17**, 341 (2005).
6. F. D. M. Haldane, Phys. Lett. A **93** 464 (1983); Phys. Rev. Lett. **50**, 1153 (1983).
7. A. Voigt, J. Richter, and P. Tomczak, Physica A **299**, 461 (2001).
8. R. F. Bishop, J. B. Parkinson, and Y. Xian, Phys. Rev. B **46**, 880 (1992).
9. D. J. J. Farnell, R. F. Bishop, and K. A. Gernoth, J. Stat. Phys. **108**, 401 (2002).
10. T. Grover and T. Senthil, arXiv:1012.5669v1 [cond-mat.str-el] (2010).
11. H. Q. Lin and V. J. Emery, Phys. Rev. B **40**, 2730 (1989).
12. V. Y. Irkhin, A. A. Katanin, and M. I. Katsnelson, J. Phys.: Condens. Matter **4**, 5227 (1992).
13. D. J. J. Farnell, K. A. Gernoth, and R. F. Bishop, Phys. Rev. B **64**, 172409 (2001).
14. S. Moukouri, J. Stat. Mech. P02002, (2006).
15. R. F. Bishop, P. H. Y. Li, R. Darradi, and J. Richter, Europhys. Lett. **83**, 47004 (2008)
16. R. F. Bishop, P. H. Y. Li, R. Darradi, J. Richter, and C. E. Campbell, J. Phys.: Condens. Matter **20**, 415213 (2008).
17. H. C. Jiang, F. Krüger, J. E. Moore, D. N. Sheng, J. Zaanen, and Z. Y. Weng, Phys. Rev. B **79**, 174409 (2009).
18. R. F. Bishop and P. H. Y. Li, Eur. Phys. J. B **81**, 37 (2011).
19. H. H. Zhao, Q. N. Chen, Z. C. Wei, M. P. Qin, G. M. Zhang, and T. Xiang, arXiv:1105.2716v1 [cond-mat.str-el] (2011).
20. M. A. de Vries, T. K. Johal, A. Mirone, J. S. Claydon, G. J. Nilson, H. M. Rønnow, G. van der Laan, and A. Harrison, Phys. Rev. B **79**, 045102 (2009).
21. Y. Kamihara, T. Watanabe, M. Hirano, and H. Hosono, J. Am. Chem. Soc. **130**, 3296 (2008).
22. F. Ma, Z.-Y. Lu, and T. Xiang, Phys. Rev. B **78**, 224517 (2008).
23. R. F. Bishop, Theor. Chim. Acta **80**, 95 (1991).

24. R. F. Bishop, in *Microscopic Quantum Many-Body Theories and Their Applications*, edited by J. Navarro and A. Polls, *Lecture Notes in Physics* **510** (Springer-Verlag, Berlin, 1998), p.1.
25. D. J. J. Farnell and R. F. Bishop, in *Quantum Magnetism*, edited by U. Schollwöck, J. Richter, D. J. J. Farnell, and R. F. Bishop, *Lecture Notes in Physics* **645** (Springer-Verlag, Berlin, 2004), p.307.
26. R. F. Bishop, P. H. Y. Li, D. J. J. Farnell, and C. E. Campbell, *Phys. Rev. B* **79**, 174405 (2009).
27. R. F. Bishop, P. H. Y. Li, D. J. J. Farnell, and C. E. Campbell, *Int. J. Mod. Phys. B* **24**, 5011 (2010); *ibid.* Erratum (2011).
28. J. Merino, R. H. McKenzie, J. B. Marston, and C. H. Chung, *J. Phys.: Condens. Matter* **11**, 2965 (1999).
29. Zheng Weihong, R. H. McKenzie, and R. R. P. Singh, *Phys. Rev. B* **59**, 14367 (1999).
30. O. A. Starykh and L. Balents, *Phys. Rev. Lett.* **98**, 077205 (2007).
31. T. Pardini and R. R. P. Singh, *Phys. Rev. B* **77**, 214433 (2008).
32. H. Kino and H. Fukuyama, *J. Phys. Soc. Japan* **65**, 2158 (1996); R. H. McKenzie, *Comments Condens. Matter Phys.* **18**, 309 (1998).
33. R. Coldea, D. A. Tennant, R. A. Cowley, D. F. McMorrow, B. Dorner, and Z. Tylczynski, *Phys. Rev. Lett.* **79**, 151 (1997).
34. H. A. Bethe, *Z. Phys.* **71**, 205 (1931).
35. J. Villain, *J. Phys. (France)* **38**, 385 (1977); J. Villain, R. Bidaux, J. P. Carton, and R. Conte, *ibid.* **41**, 1263 (1980); E. Shender, *Sov. Phys. JETP* **56**, 178 (1982).
36. R. F. Bishop, P. H. Y. Li, R. Darradi, and J. Richter, *J. Phys.: Condens. Matter* **20**, 255251 (2008).
37. R. F. Bishop, P. H. Y. Li, R. Darradi, J. Schulenburg, and J. Richter, *Phys. Rev. B* **78**, 054412 (2008).
38. R. Orbach, *Phys. Rev.* **112**, 309 (1958); C. N. Yang and C. P. Yang, *ibid.* **150**, 321 (1966); **150**, 327 (1966); R. J. Baxter, *J. Stat. Phys.* **9**, 145 (1973).
39. C. Zeng, D. J. J. Farnell, and R. F. Bishop, *J. Stat. Phys.* **90**, 327 (1998).
40. S. E. Krüger, J. Richter, J. Schulenburg, D. J. J. Farnell, and R. F. Bishop, *Phys. Rev. B* **61**, 14607 (2000).
41. D. J. J. Farnell, R. F. Bishop, and K. A. Gernoth, *Phys. Rev. B* **63**, 220402(R) (2001).
42. R. Darradi, J. Richter, and D. J. J. Farnell, *Phys. Rev. B* **72**, 104425 (2005).
43. D. Schmalfuß, R. Darradi, J. Richter, J. Schulenburg, and D. Ihle, *Phys. Rev. Lett.* **97**, 157201 (2006).
44. R. F. Bishop, P. H. Y. Li, D. J. J. Farnell, and C. E. Campbell, *Phys. Rev. B* **82**, 104406 (2010).
45. We use the program package “Crystallographic Coupled Cluster Method” (CCCM) of D. J. J. Farnell and J. Schulenburg, see <http://www-e.uni-magdeburg.de/jschulen/ccm/index.html>.
46. D. J. J. Farnell and R. F. Bishop, *Int. J. Mod. Phys. B* **22**, 3369 (2008).
47. P. M. Morse and H. Feshbach, *Methods of Theoretical Physics*, Part II (McGraw-Hill, New York, 1953).
48. C. J. Hamer, Zheng Weihong, and P. Arndt, *Phys. Rev. B* **46**, 6276 (1992).
49. Zheng Weihong, J. Oitmaa, and C. J. Hamer, *Phys. Rev. B* **43**, 8321 (1991).
50. S. R. White and D. A. Huse, *Phys. Rev. B* **48**, 3844 (1993).
51. S. Nakatsuji, Y. Nambu, H. Tonomura, O. Sakai, S. Jonas, C. Broholm, H. Tsunetsugu, Y. Qiu, and Y. Maeno, *Science* **309**, 1697 (2005).
52. J. G. Cheng, G. Li, L. Balicas, J. S. Zhou, J. B. Goodenough, Cenke Xu, and H. D. Zhou, *Phys. Rev. Lett.* **107**, 197204 (2011).
53. S. Bhattacharjee, V. B. Shenoy, and T. Senthil, *Phys. Rev. B* **74**, 092406 (2006).
54. A. Lauchli, F. Mila, and K. Penc, *Phys. Rev. Lett.* **97**, 087205 (2006).
55. H. Tsunetsugu and M. Arikawa, *J. Phys. Soc. Jpn.* **75**, 083701 (2006).
56. E. M. Stoudenmire, S. Trebst, and L. Balents, *Phys. Rev. B* **79**, 214436 (2009).
57. C. Xu, F. Wang, Y. Qi, L. Balents, and M. P. A. Fisher, arXiv:1110.3328v1 [cond-mat.str-el] (2011).
58. D. J. J. Farnell, R. F. Bishop, P. H. Y. Li, J. Richter, and C. E. Campbell, *Phys. Rev. B* **84**, 012403 (2011).
59. Y. Xian, *J. Phys.: Condens. Matter* **6**, 5965 (1994).
60. D. J. J. Farnell, J. Richter, R. Zinke and R. F. Bishop, *J. Stat. Phys.* **135**, 175 (2009).
61. B. S. Shastry and B. Sutherland, *Physica B* **108**, 1069 (1981).

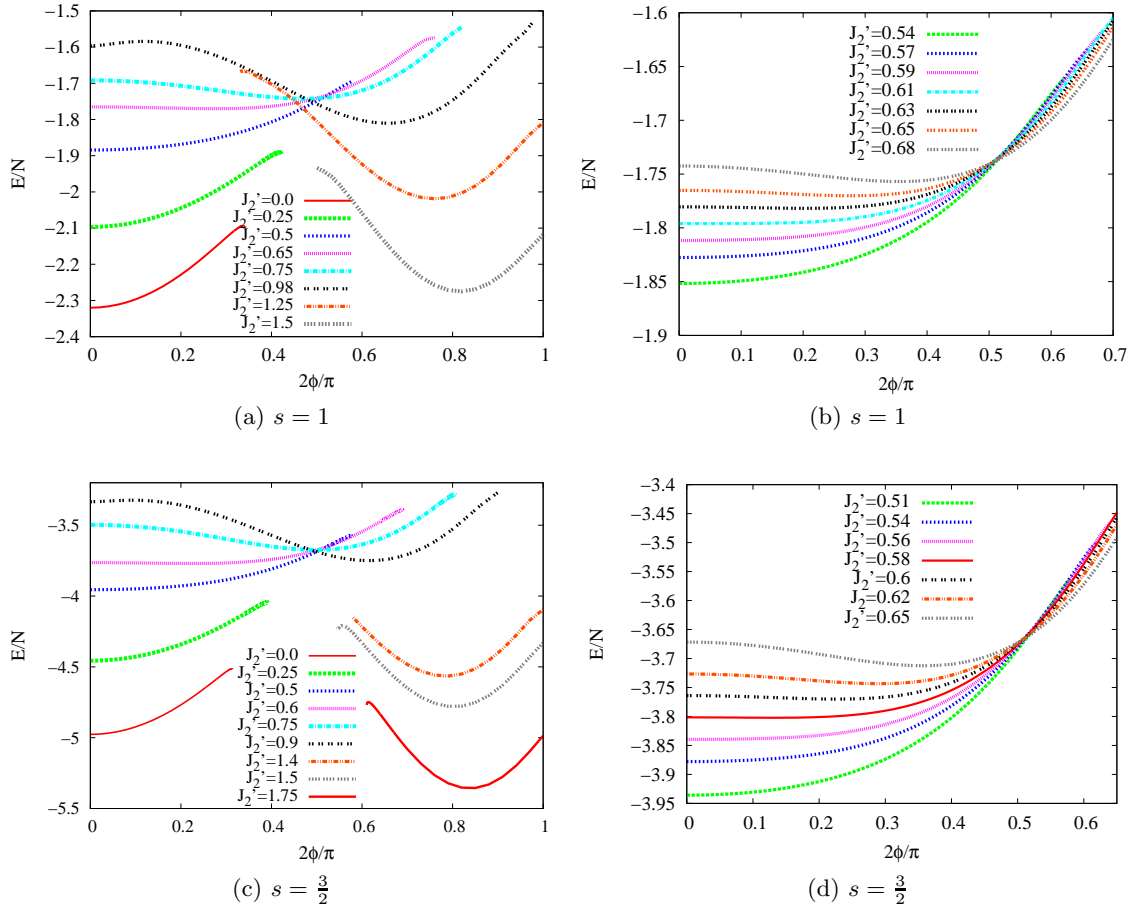


Fig. 2: (colour online) Ground-state energy per spin of the spin-1 and spin- $\frac{3}{2}$ J_1 - J_2' Hamiltonian of Eq. (1) with $J_1 = 1$, using the SUB4-4 approximation of the CCM with the spiral model state, versus the spiral angle ϕ . For the case of $s = 1$, for $J_2' \lesssim 0.610$ the only minimum is at $\phi = 0$ (Néel order), whereas for $J_2' \gtrsim 0.610$ a secondary minimum occurs at $\phi = \phi_{\text{SUB4-4}} \neq 0$, which is also a global minimum, thus illustrating the typical scenario of a second-order phase transition. Similarly, for the case of $s = \frac{3}{2}$, for $J_2' \lesssim 0.571$ the only minimum is at $\phi = 0$ (Néel order), whereas for $J_2' \gtrsim 0.571$ a secondary minimum occurs at $\phi = \phi_{\text{SUB4-4}} \neq 0$.

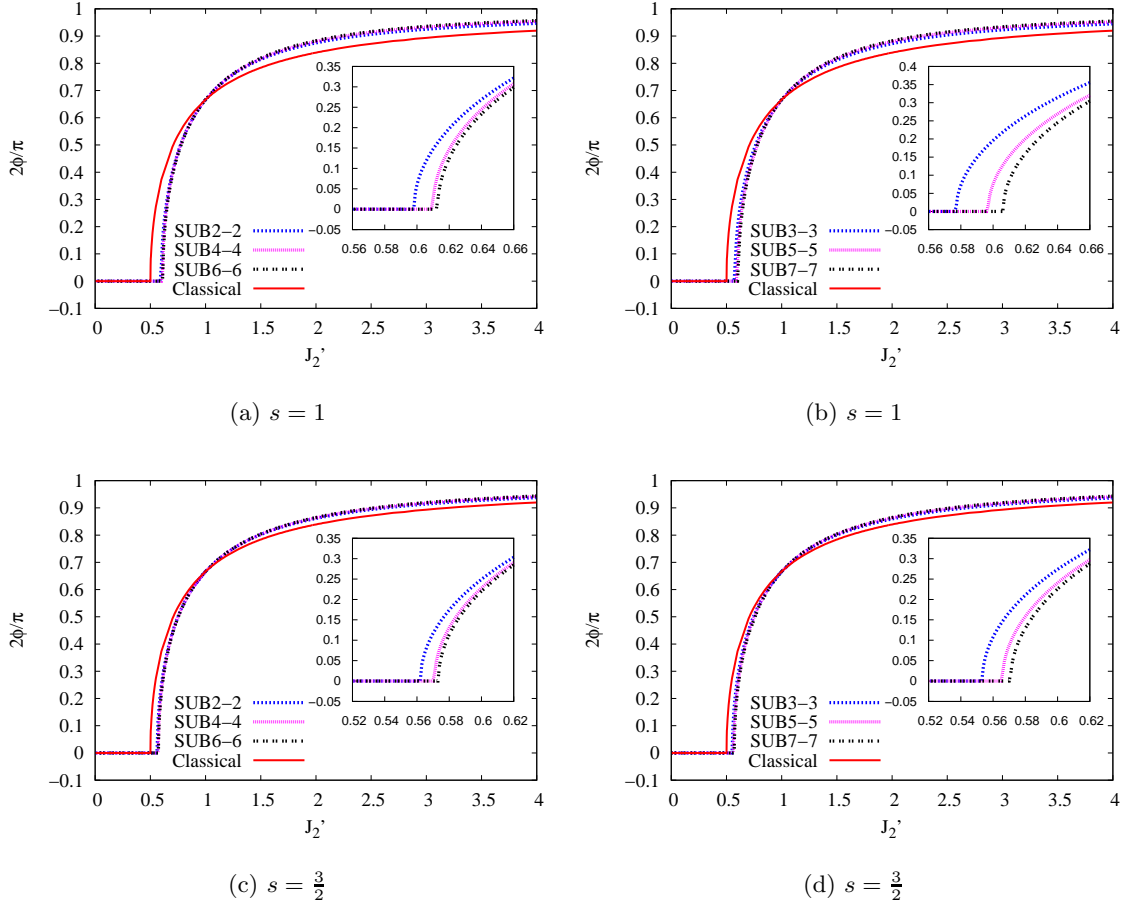


Fig. 3: (colour online) The angle $\phi_{\text{SUB}n-n}$ that minimizes the energy $E_{\text{SUB}n-n}(\phi)$ of the spin-1 and spin- $\frac{3}{2}$ J_1 - J'_2 Hamiltonian of Eq. (1) with $J_1 = 1$, in the SUB n - n approximations with $n = \{2, 4, 6\}$ and $n = \{3, 5, 7\}$, using the spiral model state, versus J'_2 . The corresponding classical result ϕ_{cl} is shown for comparison. We find in the SUB n - n quantum case a second-order phase transition (e.g., at the SUB6-6 level, at $J'_2 \approx 0.613$ for the $s = 1$ case and at $J'_2 \approx 0.574$ for the $s = \frac{3}{2}$ case), where $\phi_{\text{SUB}n-n}$ changes continuously from zero below the transition point (Néel phase) to a nonzero value above it (helical phase). The classical case has a second-order phase transition at $J'_2 = 0.5$.

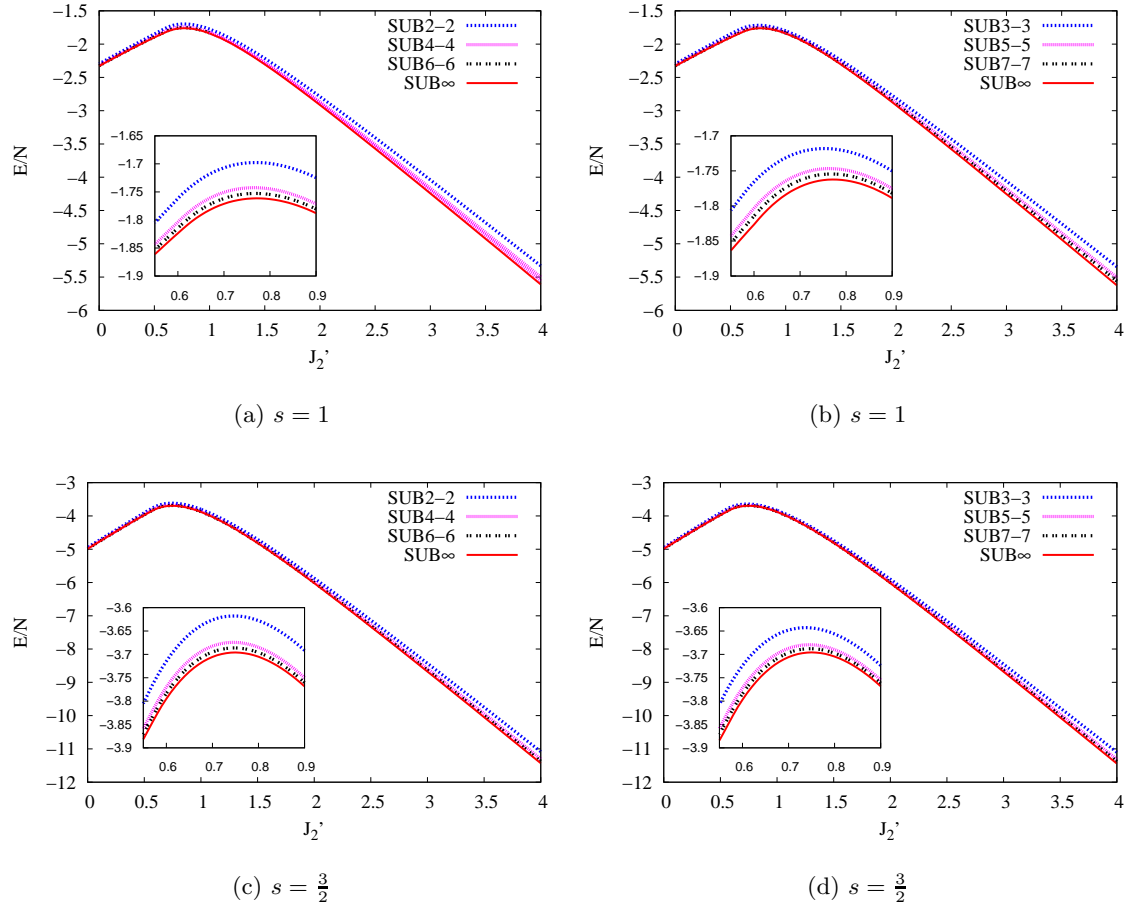


Fig. 4: (colour online) Ground-state energy per spin versus J_2' for the Néel and spiral phases of the spin-1 and spin- $\frac{3}{2}$ J_1 - J_2' Hamiltonian of Eq. (1) with $J_1 = 1$. The CCM results using the spiral model state are shown for various SUB n - n approximations ($n = \{2, 4, 6\}$) and ($n = \{3, 5, 7\}$) with the spiral angle $\phi = \phi_{\text{SUB}n-n}$ that minimizes $E_{\text{SUB}n-n}(\phi)$. We also show the $n \rightarrow \infty$ extrapolated results from using Eq. (3).

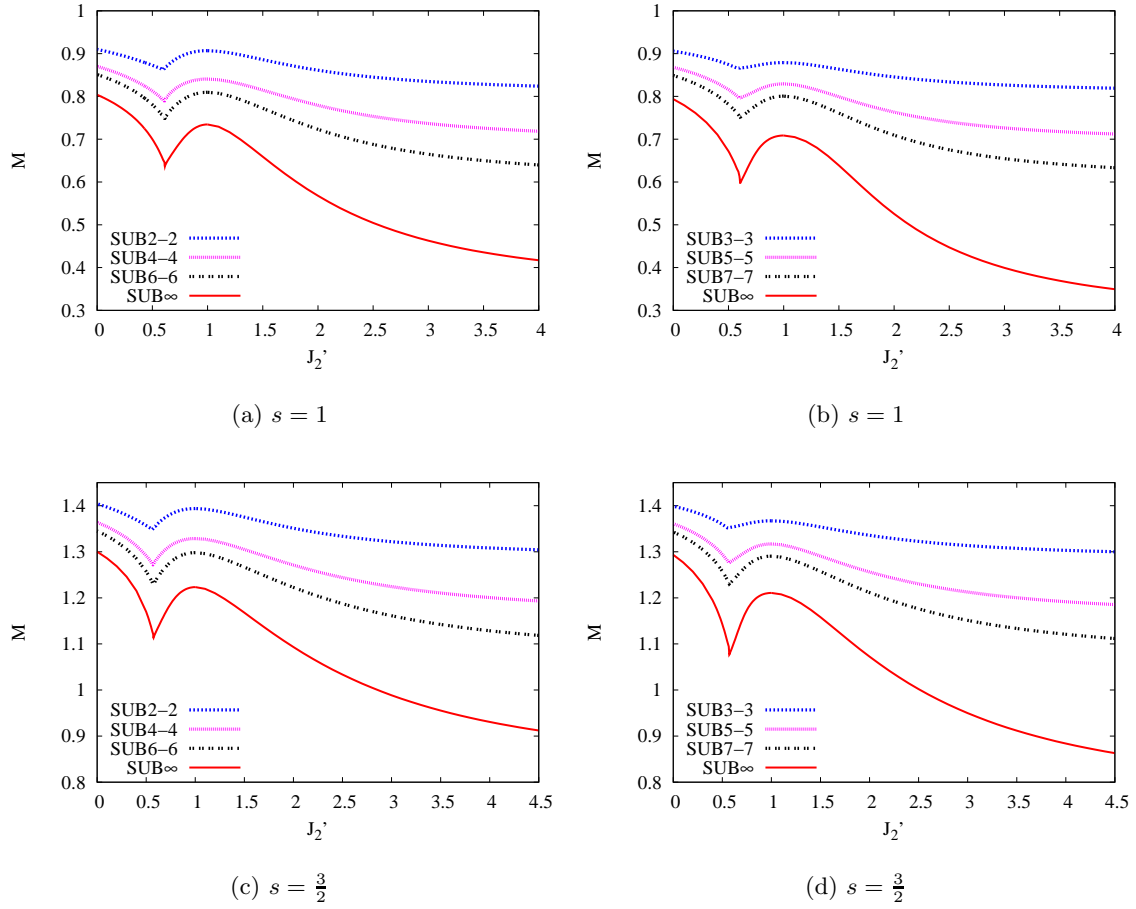


Fig. 5: (colour online) Ground-state magnetic order parameter (i.e., the average on-site magnetization) versus J_2' for the Néel and spiral phases of the spin-1 and spin- $\frac{3}{2}$ J_1 - J_2' Hamiltonian of Eq. (1) with $J_1 = 1$. The CCM results using the spiral model state are shown for various $SUBn-n$ approximations ($n = \{2, 4, 6\}$ and $n = \{3, 5, 6\}$) with the spiral angle $\phi = \phi_{SUBn-n}$ that minimizes $E_{SUBn-n}(\phi)$. We also show the $n \rightarrow \infty$ extrapolated results from using Eq. (4). The sharp minimum in the extrapolated magnetic order parameter is at $J_2' = 0.613$ ($M = 0.6367$) using $n = \{2, 4, 6\}$ and $J_2' = 0.606$ ($M = 0.5978$) using $n = \{3, 5, 7\}$ for the spin-1 case, whereas for the spin- $\frac{3}{2}$ case, the corresponding values are $J_2' = 0.574$ ($M = 1.1134$) using $n = \{2, 4, 6\}$ and $J_2' = 0.571$ ($M = 1.0766$) using $n = \{3, 5, 7\}$.

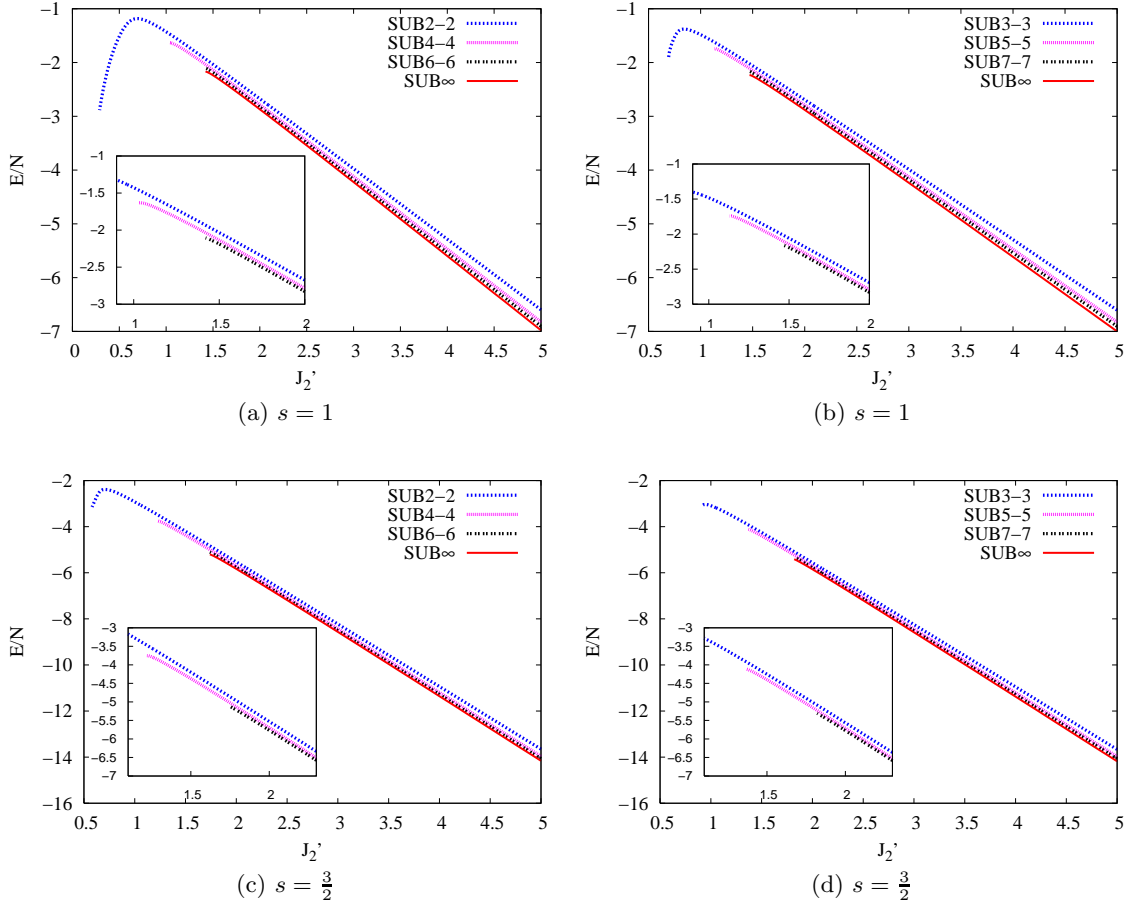


Fig. 6: (colour online) Ground-state energy per spin versus J_2' for the stripe-ordered phase of the spin-1 and spin- $\frac{3}{2}$ J_1 - J_2' Hamiltonian of Eq. (1) with $J_1 = 1$. The CCM results using the striped model state are shown for various $\text{SUB}n$ - n approximations ($n = \{2, 4, 6\}$) and ($n = \{3, 5, 7\}$). We also show the $n \rightarrow \infty$ extrapolated results from using Eq. (3).

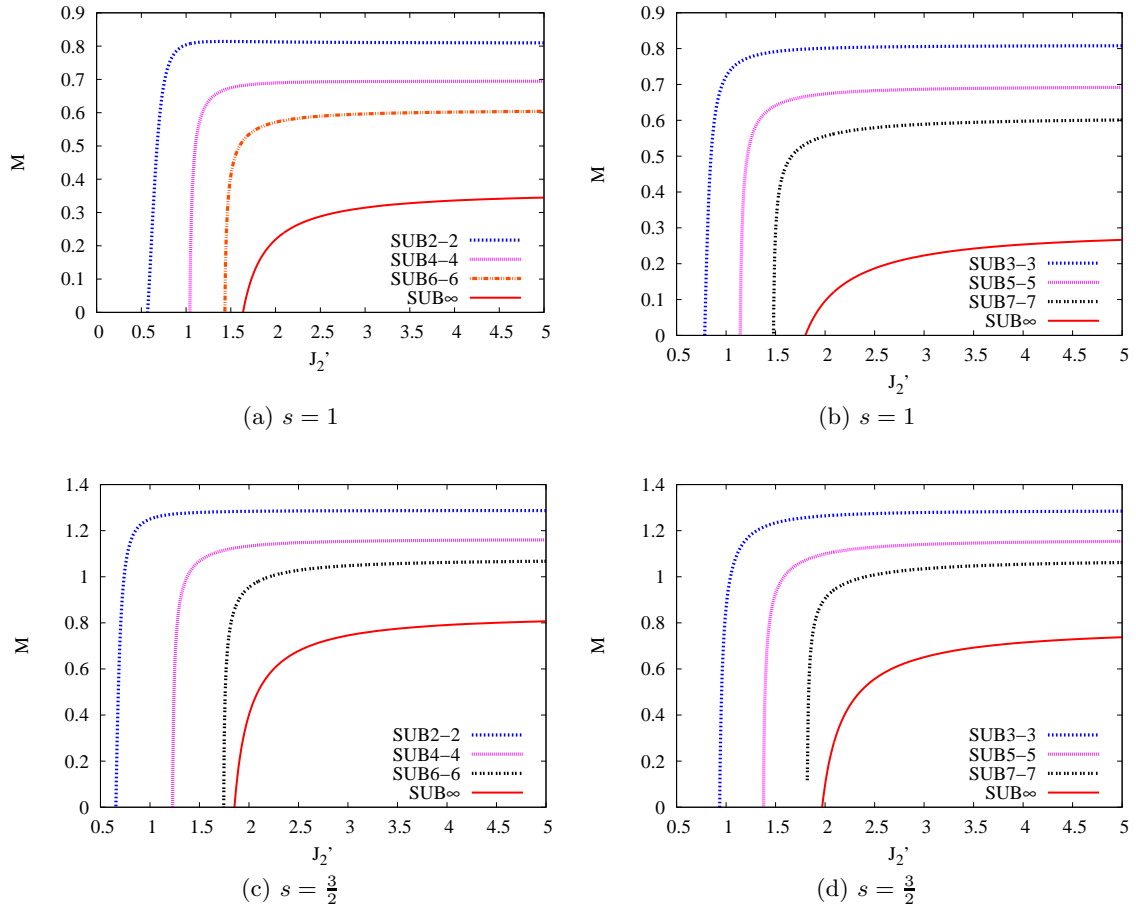


Fig. 7: (colour online) Ground-state magnetic order parameter (i.e., the average on-site magnetization) versus J_2' for the stripe-ordered phase of the spin-1 and spin- $\frac{3}{2}$ J_1 - J_2' Hamiltonian of Eq. (1) with $J_1 = 1$. The CCM results using the striped model state are shown for various SUB n - n approximations ($n = \{2, 4, 6\}$ and $n = \{3, 5, 7\}$). We also show the $n \rightarrow \infty$ extrapolated results from using Eq. (4).

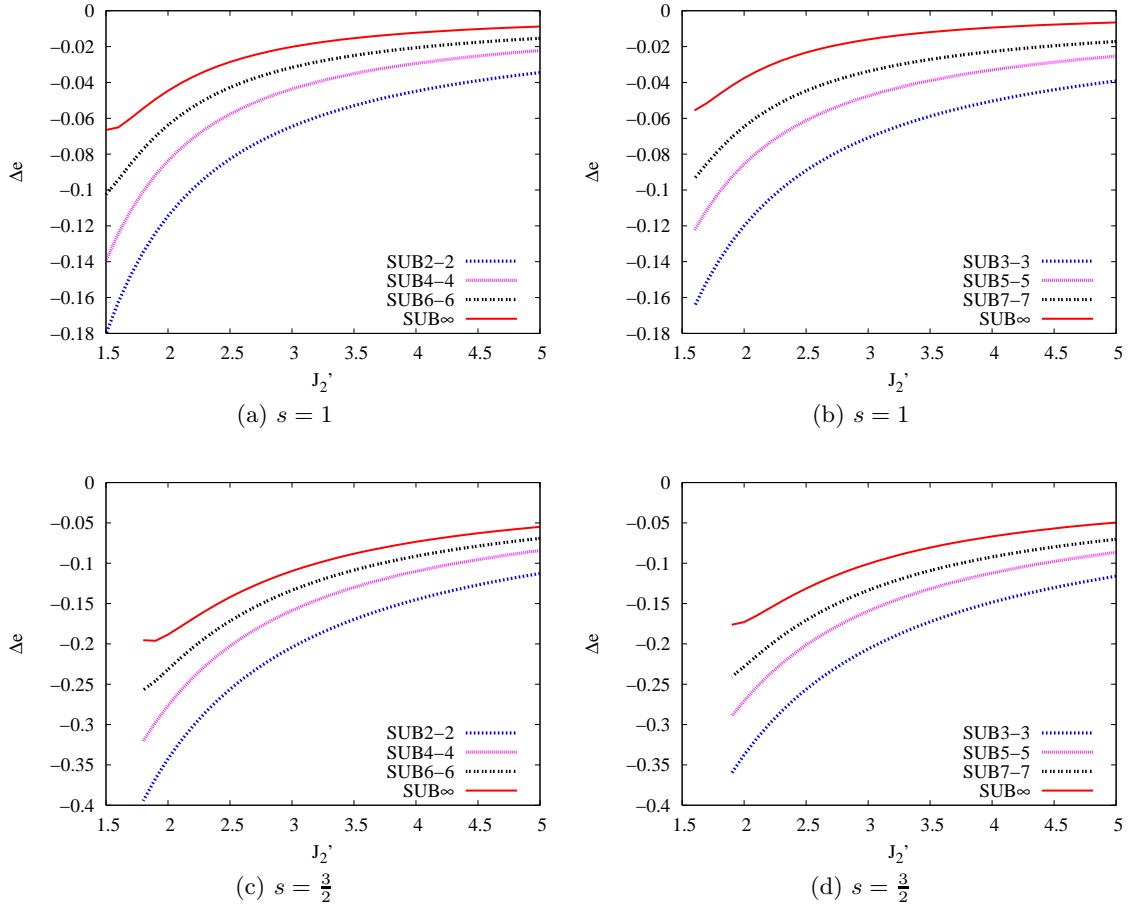


Fig. 8: (colour online) Difference between the ground-state energies per spin ($e \equiv E/N$) of the spiral and striped phases ($\Delta e \equiv e^{\text{spiral}} - e^{\text{striped}}$) versus J_2' for the spin-1 and spin- $\frac{3}{2}$ J_1 - J_2' Hamiltonian of Eq. (1) with $J_1 = 1$. The CCM results for the energy difference using both the striped and spiral model states for various SUB n - n approximations ($n = \{2, 4, 6\}$) and ($n = \{3, 5, 7\}$) are shown. We also show the $n \rightarrow \infty$ extrapolated results from using Eq. (3) for the two phases separately.

